CHINESE JOURNAL OF MECHANICAL ENGINEERING
Vol. 28, No. 5, 2015

DOI: 10.3901/CJME.2015.0703.085, available online at www.springerlink.com; www.cjmenet.com; www.cjme.com.cn

Impact of Typical Steady-state Conditions and Transient Conditions on Flow Ripple and Its Test Accuracy for Axial Piston Pump

XU Bing*, HU Min, and ZHANG Junhui

State Key Laboratory of Fluid Power Transmission and Control, Zhejiang University, Hangzhou 310027, China

Received January 29, 2014; revised January 12, 2015; accepted July 3, 2015

Abstract: The current research about the flow ripple of axial piston pump mainly focuses on the effect of the structure of parts on the flow ripple. Therein, the structure of parts are usually designed and optimized at rated working conditions. However, the pump usually has to work in large-scale and time-variant working conditions. Therefore, the flow ripple characteristics of pump and analysis for its test accuracy with respect to variant steady-state conditions and transient conditions in a wide range of operating parameters are focused in this paper. First, a simulation model has been constructed, which takes the kinematics of oil film within friction pairs into account for higher accuracy. Afterwards, a test bed which adopts Secondary Source Method is built to verify the model. The simulation and tests results show that the angular position of the piston, corresponding to the position where the peak flow ripple is produced, varies with the different pressure. The pulsating amplitude and pulsation rate of flow ripple increase with the rise of pressure and the variation rate of pressure. For the pump working at a constant speed, the flow pulsation rate decreases dramatically with the increasing speed when the speed is less than 27.78% of the maximum speed, subsequently presents a small decrease tendency with the speed further increasing. With the rise of the variation rate of speed, the pulsating amplitude and pulsation rate of flow ripple increase. As the swash plate angle augments, the pulsating amplitude of flow ripple increases, nevertheless the flow pulsation rate decreases. In contrast with the effect of the variation of pressure, the test accuracy of flow ripple is more sensitive to the variation of speed. It makes the test accuracy above 96.20% available for the pulsating amplitude of pressure deviating within a range of ±6% from the mean pressure. However, with a variation of speed deviating within a range of ±2% from the mean speed, the attainable test accuracy of flow ripple is above 93.07%. The model constructed in this research proposes a method to determine the flow ripple characteristics of pump and its attainable test accuracy under the large-scale and time-variant working conditions. Meanwhile, a discussion about the variation of flow ripple and its obtainable test accuracy with the conditions of the pump working in wide operating ranges is given as well.

Keywords: axial piston pump, flow ripple, test accuracy, steady-state condition, transient condition, wide operating ranges

1 Introduction

More and more restrictive regulations and standards cause developers of hydraulic pump to think about reducing the noise and improving the efficiency of axial piston pump under a large-scale working condition. As it is well known, the flow ripple is one of the most important noise sources of axial piston pump. In order to design or optimize a pump with low-level noise under different working conditions, it is the first necessity to gain an insight into how the flow ripple is affected by the different working conditions.

The working conditions of pump can be basically divided into steady-state conditions and transient conditions, mainly involving variant characteristics of delivery pressure, speed and swash plate angle. The impact of different kinds of working conditions on flow ripple can be discussed from the following two aspects: the impact on the variation of flow ripple and the impact on the test accuracy of flow ripple due to the complexity of test method for the flow ripple.

In most cases, due to the conventional assumption of axial piston pump usually working at specific design point, more attention about the influencing factors on the variation of flow ripple has been focused on other factors as follows, rather than the large-scale time-variant working conditions. The effect of valve-plate parameters on the flow ripple, such as the geometry and position of relief groove or the damping hole in valve plate, has been widely studied in recent years[1–10]. EDGE, et al[11], in 1989 developed a simulation model, accounting for the influence of oil momentum in the valve plate region on the flow ripple. MANRING[12] analyzed the flow ripple of piston pump with different piston number in 2000, which showed that a pump designed with an even number of pistons may be as feasible as one that is designed with an odd number of pistons from a flow ripple point of view. MA, et al[13],

* Corresponding author. E-mail: bxu@zju.edu.cn
Supported by National Basic Research Program of China (973 Program, Grant No. 2014CB046403), and National Key Technology R&D Program of the Twelfth Five-year Plan of China (Grant No. 2013BAF07B01)

investigated the effect of compressibility of hydraulic oil on flow ripple in 2010, and pointed out that the compression ripple accounts for about 88% of the total flow ripple of pump. SHI, et al[14] and LEI, et al[15], investigated the discharge flow ripple of pump with conical cylinder block in 2010, concluded that the cylinder block cone angle has a significant impact on the discharge flow ripple, and utilizing a conical cylinder block design is more feasible than cylindrical cylinder block from a flow ripple point of view. The influence of cross angel of swash plate on the flow ripple of pump were investigated by MA, et al[16] in 2010, WEI, et al[17] in 2012, and SONG, et al[18] in 2013. ERICSON[19] investigated the effect of non-uniform placement of the pistons on the flow ripple of pump in 2009. The effect of piston travel trajectory on the flow ripple of pump was investigated by MEHTA, et al[20] in 2010. BERGADA, et al[21], investigated the impact of leakages in all piton pump gaps on the output flow ripple in 2012, and concluded that regardless of the percentage increase in clearance, the shape of the temporal output flow ripple remains constant, nevertheless the pump outflow decreases about 6% when the magnitude of the clearances doubles. SONG, et al[22], examined the parameters of pre-compression volume on the flow ripple of pump in 2013. ZHANG, et al[23], analyzed the flow ripple of pump with pressure equalization mechanism composed of check valve and pressure recuperation chamber in 2013. LISELOTT[24] investigated the effect of swash plate oscillations due to the internal piston forces on the outlet flow pulsations of pump in 2013.

Simultaneously, some results about the variation of flow ripple with the working conditions, which obtained by the simulation method or test method, have been provided in previous researches. In 1990, test result with respect to different delivery pressure, attained by the Secondary Source Method, was given by EDGE, et al[25–26]. The result shows that the reverse flow is the main reason for affecting the flow ripple. In addition, the amplitude of the reverse flow increases with delivery pressure. KASSEM, et al[27], computed a series of flow ripple with respect to different delivery pressure in 2000. In 2007, the flow ripple was tested by Two-micro Phone Method and the results with respect to different delivery pressure were brought forward by JOHANSSON, et al[28]. Based upon the results, it can be seen that the amplitude of flow ripple increases with the delivery pressure. ZHANG, et al[29], presented the research result that the flow ripple amplitude is getting higher with the rise of swash plate angle in 2009, nevertheless the reason of the result was not explained, furthermore, the variation of the flow pulsation rate with the swash plate angle was not given in his research as well. The flow ripple generated by pump with complicated pipe was investigated by SONG, et al[30–31] under different pressure conditions in 2012 and 2014.

From the above review about the impact of working conditions on the flow ripple, the considerable emphasis has been mainly placed on the impact of delivery pressure on the flow ripple. Nevertheless the flow ripple is also greatly affected by the different time-varying speed, swash plate angle, and different kinds of transient conditions. In order to attain accurate test result of flow ripple, the impact of the working conditions of test circuit on the test accuracy of flow ripple should be discussed as well.

In this research, first a detailed simulation model is proposed, which takes the following factors into account: the compressibility of fluid, the movement of piston and oil films within key friction pairs, the structure of relief groove and the inertia of oil in the relief groove. Subsequently, the test results of flow ripple attained by the Secondary Source Method are provided and the confirmation of the simulation model is done. Third, the effect on the flow ripple and its test accuracy by variant typical steady-state and transient working conditions obtained from simulation and test are analyzed and discussed. At last, some conclusions are drawn.

2 Description of the CFD Model

2.1 Simulation model

Fig. 1 shows the numerical computation model, including the fluid zone in axial piston pump and pipe. The leakage of the oil film in piston/cylinder pair, slipper/swash-plate pair and valve-plate/cylinder pair are taken into account in the model.

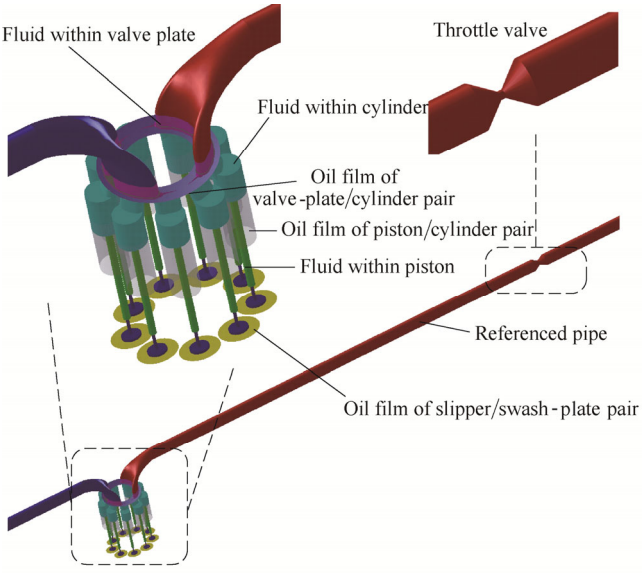

Fig. 1. Numerical computation model

The terminal impedance of numerical computation model is simulated by a throttle valve, the throttling area is determined by Eq. (1):

$$A_v = \frac{q}{C_v}\sqrt{\frac{\rho}{2\Delta P}}, \tag{1}$$

where C_v denotes the flow coefficient, ρ denotes the density

of hydraulic oil, q denotes the flowrate, ΔP denotes the pressure difference.

In order to attain accurate results, the flow state of fluid in pump and pipe should be laminar flow, which can be determined by Reynolds number. The Reynolds number is calculated by Eq. (2):

$$Re=\frac{4\rho VA_r}{l_c\mu}, \tag{2}$$

where V denotes the velocity of fluid, A_r denotes the effective sectional area of flow, l_c denotes the wetted perimeter, and μ denotes the fluid viscosity.

The finite volume method is adopted in the computation of numerical model by a commercial CFD software. In each control volume, the fluid follows the mass conservation law, momentum conservation law and energy conservation law as follows.

The conservation equation of mass:

$$\frac{\partial\rho}{\partial t}+\frac{\partial(\rho u)}{\partial x}+\frac{\partial(\rho v)}{\partial y}+\frac{\partial(\rho w)}{\partial z}=0, \tag{3}$$

The conservation equation of momentum:

$$\frac{\partial(\rho u)}{\partial t}+\frac{\partial(\rho uu)}{\partial x}+\frac{\partial(\rho uv)}{\partial y}+\frac{\partial(\rho uw)}{\partial z}=\frac{\partial}{\partial x}\left(\mu\frac{\partial u}{\partial x}\right)+\frac{\partial}{\partial y}\left(\mu\frac{\partial u}{\partial y}\right)+\frac{\partial}{\partial z}\left(\mu\frac{\partial u}{\partial z}\right)-\frac{\partial P}{\partial x}+S_u, \tag{4}$$

$$\frac{\partial(\rho v)}{\partial t}+\frac{\partial(\rho vu)}{\partial x}+\frac{\partial(\rho vv)}{\partial y}+\frac{\partial(\rho vw)}{\partial z}=\frac{\partial}{\partial x}\left(\mu\frac{\partial v}{\partial x}\right)+\frac{\partial}{\partial y}\left(\mu\frac{\partial v}{\partial y}\right)+\frac{\partial}{\partial z}\left(\mu\frac{\partial v}{\partial z}\right)-\frac{\partial P}{\partial y}+S_v, \tag{5}$$

$$\frac{\partial(\rho w)}{\partial t}+\frac{\partial(\rho wu)}{\partial x}+\frac{\partial(\rho wv)}{\partial y}+\frac{\partial(\rho ww)}{\partial z}=\frac{\partial}{\partial x}\left(\mu\frac{\partial w}{\partial x}\right)+\frac{\partial}{\partial y}\left(\mu\frac{\partial w}{\partial y}\right)+\frac{\partial}{\partial z}\left(\mu\frac{\partial w}{\partial z}\right)-\frac{\partial P}{\partial z}+S_w. \tag{6}$$

The conservation equation of energy:

$$\frac{\partial(\rho T)}{\partial t}+\frac{\partial(\rho uT)}{\partial x}+\frac{\partial(\rho vT)}{\partial y}+\frac{\partial(\rho wT)}{\partial z}=\frac{\partial}{\partial x}\left(\frac{\xi}{c_p}\frac{\partial T}{\partial x}\right)+\frac{\partial}{\partial y}\left(\frac{\xi}{c_p}\frac{\partial T}{\partial y}\right)+\frac{\partial}{\partial z}\left(\frac{\xi}{c_p}\frac{\partial T}{\partial z}\right)+S_T, \tag{7}$$

where u, v and w denote the velocity component in x-y-z three directions, ξ denotes the heat transmission coefficient, S_u, S_v, S_w and S_T denote the corresponding source term, and c_p denotes the specific heat capacity.

The hydraulic oil within numerical model is considered as compressible fluid. The density is determined by Eq. (8), ε denotes the bulk modulus:

$$\rho=\frac{\varepsilon\rho_0}{\varepsilon-P-P_0}, \tag{8}$$

The sound velocity should be introduced into the numerical computation of compressible fluid, the sound velocity c_0 is calculated by Eq. (9):

$$c_0=\sqrt{\frac{\varepsilon-(P-P_0)}{\rho_0}}. \tag{9}$$

The temperature distribution of fluid within numerical model is calculated by Eq. (7). The viscosity of fluid is affected by temperature T and pressure P. The viscosity-pressure-temperature relationship proposed by ROELANDS[32] is employed in the analysis. Fluid uses hydraulic oil L-HM46. Eq. (10) is got from the Roelands viscosity-pressure-temperature equation and the measured data of viscosity vs temperature of L-HM46 oil[33]:

$$\mu=0.0457\exp\left\{6.58\times\left[(1+5.1\times10^{-9}P)^{2.3\times10^{-8}}\times\left(\frac{T-138}{303-138}\right)^{-1.16}-1\right]\right\}. \tag{10}$$

2.2 Boundary conditions

In order to attain accurate results, appropriate boundary conditions should be set in the simulation. Based upon the operational principle of axial piston pump, the input port of the CFD model is pressure inlet, and the output port is pressure outlet.

As an inherent attribute of pump, the kinematic flow ripple is needed to be taken into account in the simulation model. The boundary condition describing the movement of fluid within cylinder, piston and slipper is presented in Fig. 2.

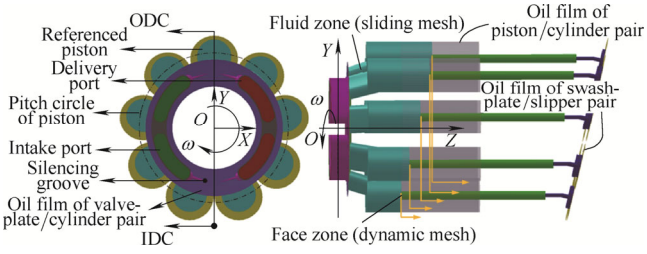

Fig. 2. Boundary conditions describing the movement of fluid

In addition, the leakage flowrate is taken into account in the simulation model in the form of oil film with extra-thin thickness, as Fig. 2 shows. The reciprocating motion of fluid within each piston chamber and piston, as well as the oil film of piston/cylinder pair, is molded by the dynamic grid with moving and deforming mesh. The rotary motion of fluid zone, including the fluid within cylinder, piston chamber, piston and slipper, as well as the oil film within

piston/cylinder pair and slipper/swash-plate pair, is modeled by sliding mesh.

The oil film connects with the fluid in the pump case, therefore the boundary condition of oil film is set as pressure outlet with the value of pressure in the case. According to the measuring data, the temperature in the input port and output port of the model is set to 40 °C, and the temperature in the oil film is empirically set to 60 °C.

In steady-state conditions, the pressure of input port and output port of the model is set to constant. Nevertheless in transient conditions, the pressure and working speed change with time frequently to meet the requirement of main circuit. The typical transient conditions are periodical change and instantaneous change, as Fig. 3 shows. The periodical change of pressure is defined by Eq. (11):

$$P(t) = P_m + P_{am}\sin(\psi_p t + \varphi_p), \tag{11}$$

where P_m denotes the mean pressure, $2P_{am}$ denotes the pulsating amplitude of pressure, ψ_p denotes the frequency, φ_p denotes the initial phase angle.

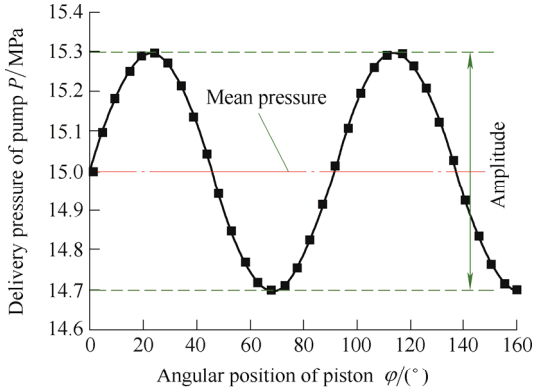

(a) Periodical change

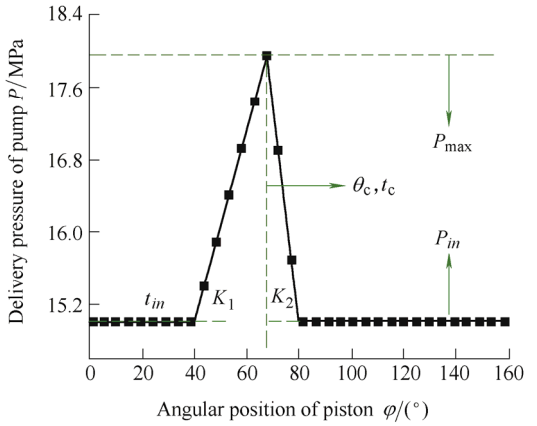

(b) Instantaneous change

Fig. 3. Typical transient conditions of delivery pressure

Assume the pressure first increases rapidly and then decreases rapidly, the rate of pressure variation is K_1 and K_2. The peak pressure is $P_{\max}$ at time t_c, and the pressure is P_{in} at time t_{in} and t_{fi}, the transient change of pressure can be defined by Eq. (12):

$$\begin{cases} P(t) = \dfrac{P_{in} - P_{\max}}{t_{in} - t_c}(t - t_{in}) + P_{in}, & t_{in} \leqslant t \leqslant t_c, \\ P(t) = \dfrac{P_{in} - P_{\max}}{t_{fi} - t_c}(t - t_{fi}) + P_{in}, & t_c \leqslant t \leqslant t_{fi}, \\ P(t) = P_{in}, & t \leqslant t_{in} \ \text{ or } \ t \geqslant t_{fi}. \end{cases} \tag{12}$$

The periodical variation of speed is defined by the following Eq. (13):

$$\omega(t) = \omega_m + \omega_{am}\sin(\psi_\omega t + \varphi_\omega), \tag{13}$$

where ω_m denotes the mean speed, $2\omega_{am}$ denotes the pulsating amplitude of speed, ψ_ω denotes the frequency and φ_ω denotes the initial phase angle.

The velocity of piston v_p is recomputed by Eq. (14) due to the changed speed:

$$\begin{aligned} v_p = {} & R(\omega_m + \omega_{am}\sin(\psi_\omega t + \varphi_\omega))\tan\beta \times \\ & \sin((\omega_m + \omega_{am}\sin(\psi_\omega t + \varphi_\omega)) \cdot t). \end{aligned} \tag{14}$$

The instantaneous variation of speed is defined by the following Eq. (15)–Eq. (18).

When $t_0 \leqslant t \leqslant t_{in}$,

$$\begin{cases} \omega(t) = \omega_0 : \text{ constant speed}, \\ v_p = R\omega_0 \tan\beta \sin(\omega_0 t) : \text{piston velocity}. \end{cases} \tag{15}$$

When $t_{in} \leqslant t \leqslant t_c$,

$$\begin{cases} \omega(t) = \omega_{01} + k_{\omega 1} t : \text{ speed}, \\ v_p = R(\omega_{01} + k_{\omega 1} t)\tan\beta \sin(k_{\omega 1} t^2 + \omega_{01} t + C_1), \\ C_1 = \int_{t_0}^{t_{in}} \omega \mathrm{d}t : \text{piston velocity}. \end{cases} \tag{16}$$

When $t_c \leqslant t \leqslant t_{fi}$,

$$\begin{cases} \omega(t) = \omega_{02} + k_{\omega 2} t : \text{speed}, \\ v_p = R(\omega_{02} + k_{\omega 2} t)\tan\beta \sin(k_{\omega 2} t^2 + \omega_{02} t + C_2), \\ C_2 = \int_{t_0}^{t_{in}} \omega \mathrm{d}t + \int_{t_{in}}^{t_c} (\omega_{01} + k_{\omega 1} t)\mathrm{d}t : \text{piston velocity}. \end{cases} \tag{17}$$

When $t \geqslant t_{fi}$,

$$\begin{cases} \omega(t) = \omega_0 : \text{ constant speed}, \\ v_p = R\omega_0 \tan\beta \sin(\omega_0 t + C_3) : \text{piston velocity}, \\ C_3 = \int_{t_0}^{t_{in}} \omega \mathrm{d}t + \int_{t_{\mathrm{in}}}^{t_c} (\omega_{01} + k_{\omega 1} t)\mathrm{d}t + \int_{t_c}^{t_{fi}} (\omega_{02} + k_{\omega 2} t)\mathrm{d}t. \end{cases} \tag{18}$$

Where R denotes the pitch circle radius of piston, β denotes the swash plate angle, ω_{01} and ω_{02} denote the initial speed,

$k_{\omega 1}$ and $k_{\omega 2}$ denote the variation rate of speed.

3 Test Method and Test Bed

The flow ripple of pump in this research is tested by the Secondary Source Method, which is a method adopted by ISO for determining the flow ripple of hydraulic pump with large flowrate and high frequency. The pump is assumed as a power in which the source flowrate and source impedance are connected in parallel. The flow ripple of tested pump is computed by the pressure ripple tested by the pressure transducer along the referenced pipe. The schematic of test method and the test bed are given in Fig. 4 and Fig. 5.

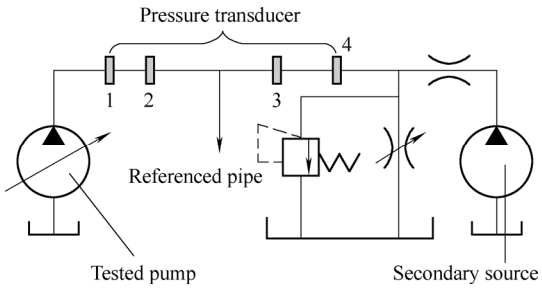

Fig. 4. Schematics for Secondary Source Method

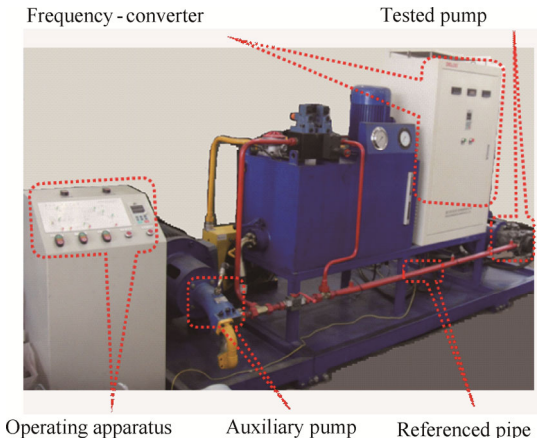

Fig. 5. Test bed of Secondary Source Method

In order to attain the source flowrate, the source impedance should be computed first by the tested pressure ripple when tested pump and auxiliary pump adopted as the secondary source running simultaneously. Then the source flowrate can be computed by source impedance and pressure ripple when tested pump runs only.

For the tested i order harmonic of secondary source, the source impedance Z_s of tested pump can be calculated by Eq. (19)[34–35]:

$$Z_{s,i} = Z_0 \frac{t_2 s_{1,1} - t_1 s_{2,1} + t_1 s_{2,2} - t_2 s_{1,2}}{t_2 s_{1,1} - t_1 s_{2,1} - t_1 s_{2,2} + t_2 s_{1,2}}, \tag{19}$$

where $s_{k,l}$ and t_k, as Eq. (20)–Eq. (23) show, are calculated by the tested pressure ripple $P_{m,i}$, which denotes the i order harmonic of pressure ripple tested by No. m pressure transducer.

$$s_{k,l} = \sum_{m=1}^{3} [\overline{f_k(x_m)} f_l(x_m)], \tag{20}$$

$$t_k = \sum_{m=1}^{3} [P_{m,i} \overline{f_1(x_m)}], \tag{21}$$

$$f_1(x) = \exp(-r_{sf} x), \tag{22}$$

$$f_2(x) = \exp(r_{sf} x). \tag{23}$$

The source flowrate Q_s is computed by Eq. (24)[34–35]:

$$P_X = Q_S \frac{Z_0 Z_S}{Z_0 + Z_S} \frac{\exp(-r_{sf} x) + \rho_T \exp[-r_{sf}(2l_p - x)]}{1 - \rho_S \rho_T \exp(-2 r_{sf} l_p)}, \tag{24}$$

where Z_0 denotes the pipeline characteristic impedance, r_{sf} is the transfer function, ρ_T denotes the termination reflection coefficient, l_p denotes the length of referenced pipe, and ρ_s denotes the source reflection coefficient.

The comparison between test results and simulation results is given in Fig. 6.

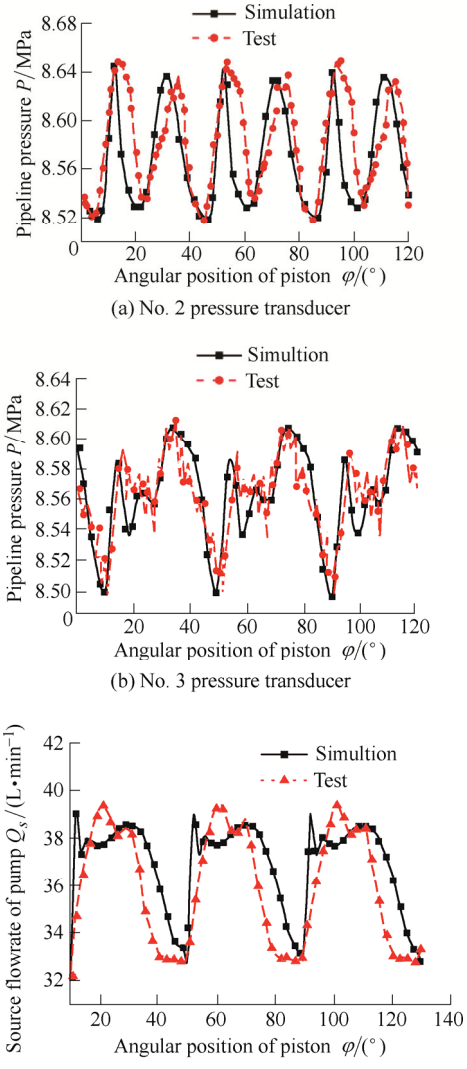

Fig. 6. Comparison between simulation results and test results

From Fig. 6, it can be seen that the test results agree well with the simulation results, and the prediction accuracy of simulation model can reach 95%. Nevertheless there are also some differences in some positions, the deviation between simulation and experiment may derive from the simplification of numerical model which does not consider all the nonlinear parameter effects. It can be concluded that the numerical model can be used to analyze the impact of variant working conditions on the flow ripple and its test accuracy.

4 Results and Discussion

The fluid-borne noise of axial piston pump is mainly affected by the flow ripple in the delivery port, which is affected by the different kinds of working conditions.

4.1 Flow ripple under steady-state conditions

4.1.1 Effect of delivery pressure

The results about the effect of delivery pressure on the flow ripple are given in Fig. 7, attained at the following working conditions: the input pressure is 2 MPa, the speed is 1000 r/min and the swash plate angle is 13°.

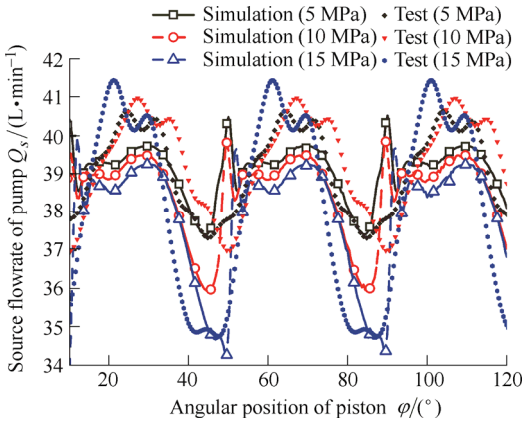

Fig. 7. Flow ripple with respect to different delivery pressure

As Fig. 7 shows, the simulation results agree well with the test results on the whole, although the tested peak flowrate is a little greater than the simulated peak flowrate. In order to analyze the effect of delivery pressure on flow ripple and the production mechanism of peak flow ripple with respect to different delivery pressure, the evaluation parameters, such as minimum flowrate, maximum flowrate, flow pulsation rate, flowrate difference and mean flowrate are given in Fig. 8. The flowrate difference and flow pulsation rate are got respectively by Eq. (25) and Eq. (26):

$$Q_{\text{sdif}} = Q_{s\max} - Q_{s\min}, \tag{25}$$

$$\delta = \frac{Q_{\text{sdif}}}{Q_{\text{sm}}}, \tag{26}$$

where Q_{smax} denotes the maximum flowrate, Q_{smin} denotes the minimum flowrate, Q_{sdif} denotes the flowrate difference, Q_{sm} denotes the mean flowrate, δ denotes the flow pulsation rate.

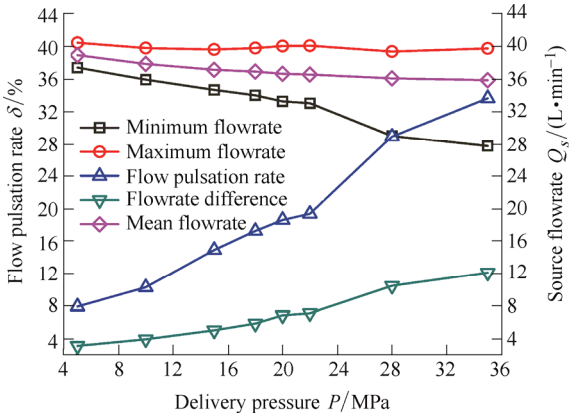

Fig. 8. Evaluation parameters of flow ripple with pressure

Based upon Fig. 8, it can be seen that the flow pulsation rate and flowrate difference increase with the rise of delivery pressure. On the contrary, the minimum flowrate and mean flowrate decrease with the delivery pressure due to the rise of leakage. The peak flow ripple with respect to different pressure is given in Fig. 9.

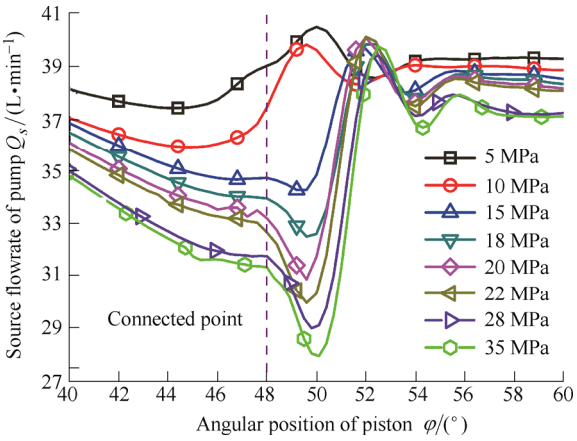

Fig. 9. Peak flow ripple with respect to delivery pressure

Fig. 9 shows that the angular position of piston, where the peak flow ripple is produced, including the minimum flowrate and the maximum flowrate, varies with the different delivery pressure. In the case that the delivery pressure is equal to or greater than 15 MPa, the minimum flowrate is produced after the piston chamber connecting directly with the pump delivery port (48°). Nevertheless when the delivery pressure is 5 MPa and 10 MPa, the minimum flowrate is produced before the piston chamber connecting directly with the pump delivery port. The main reason is that as the augment of delivery pressure, the needed amount of reverse flow increases, which is used for the pre-pressure of oil within piston chamber rising to the corresponding delivery pressure. When the delivery pressure is 5 MPa and 10 MPa, the amount of reverse flow is sufficient for the pre-pressure of oil before the piston chamber connecting directly with the delivery port.

Nevertheless as the delivery pressure further increases, the amount of reverse flow gradually can't satisfy the pre-pressure of oil before the piston chamber connecting directly with the delivery port. Fig. 9 also shows that the minimum flowrate decreases with the rise of pressure.

4.1.2 *Effect of speed*

The transition process of piston chamber rotating between suction side and discharge side of valve plate is affected by the speed, which influences the flow ripple greatly. Comparison of flow ripple with respect to different speed is given in Fig. 10. The results are obtained at the following working conditions: the suction pressure of pump is 2 MPa, the delivery pressure is 15 MPa and the swash plate angle is 13°.

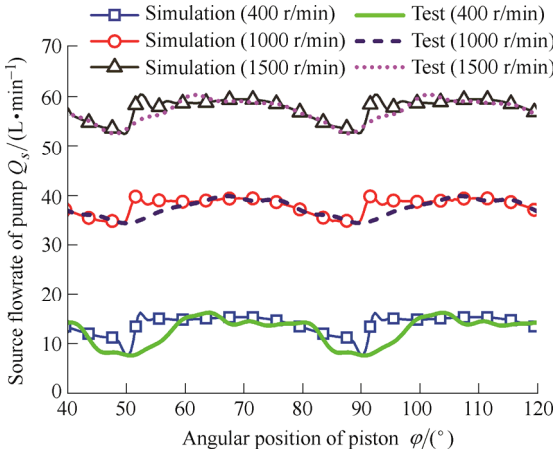

Fig. 10. Flow ripple with respect to different speed

As Fig. 10 shows, the two groups of results attained by simulation and test agree well with each other. In order to attain the effect of speed on the flow ripple, the evaluation parameters are given in Fig. 11.

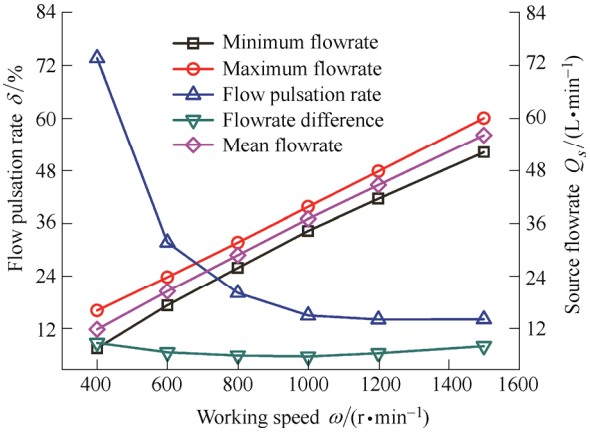

Fig. 11. Evaluation parameters of flow ripple with speed

It can be seen from Fig. 11 that the minimum flowrate, maximum flowrate and mean flowrate of pump increase with speed. The flowrate difference and the mean flowrate almost have the same order of magnitude at the speed of 400 r/min, however, as the speed further increases, the order of magnitude of mean flowrate is gradually far greater than the order of magnitude of flowrate difference. According to Eq. (26), due to the great increase rate of mean flowrate Q_{sm} and the small variation range of flowrate difference Q_{sdif} with speed, the flow pulsation rate decreases dramatically with the rise of speed when the speed is less than 1000 r/min (27.78% of the maximum allowable speed), subsequently presents a small decrease tendency with the speed further increasing.

4.1.3 *Effect of swash plate angle*

For variable displacement pump, the swash plate angle varies following the requirement of flowrate of main circuit. When the delivery pressure is 15 MPa, the speed is 1000 r/min, the flow ripple of pump with respect to different swash plate angle is given in Fig. 12. The corresponding pulsating amplitude and flow pulsation rate is given in Fig. 13.

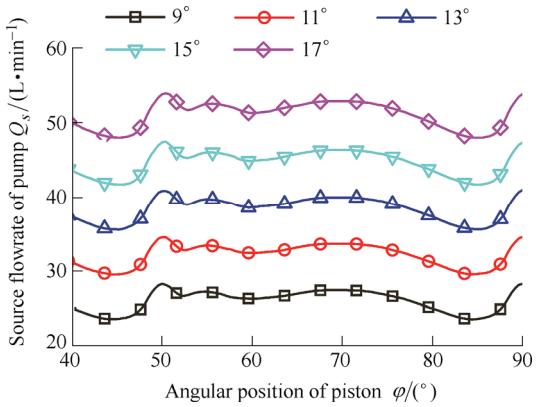

Fig. 12. Flow ripple with respect to different swash plate angle

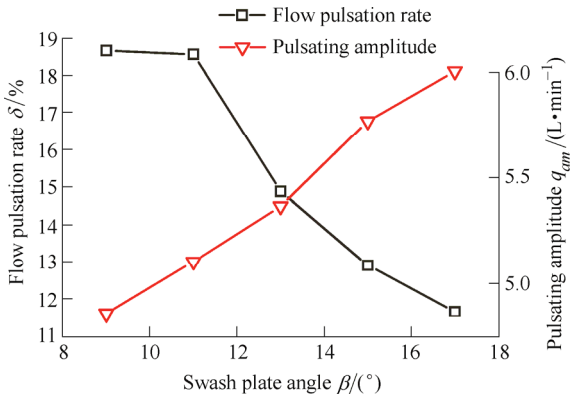

Fig. 13. Pulsating amplitude and pulsation rate of flow ripple with swash plate angle

As Fig. 12 and Fig. 13 show, with the rise of swash plate angle, the pulsating amplitude of flow ripple increases, nevertheless the flow pulsation rate decreases. The reason is that, the fluid volume within piston chamber and the reverse flow increase with the rise of swash plate angle, which results in the augment of pulsating amplitude of flow ripple, nevertheless the output flowrate of pump increases faster than the pulsating amplitude of flow ripple, thus

causing the decrease of flow pulsation rate with the swash plate angle.

4.2 Flow ripple under transient conditions

4.2.1 Effect of pressure varying periodically

Actually the delivery pressure of pump varies periodically due to the inherent pulsating characteristics of flowrate. In the boundary condition of simulation, two cases are studied according to Eq. (11). In case 1, the mean pressure is set to 15 MPa, the pulsating amplitude is respectively set to 0.6 MPa, 1.2 MPa and 1.8 MPa, the corresponding source flowrate of pump is given in Fig. 14. In case 2, the mean pressure is 35 MPa, the pulsating amplitude is respectively set to 1.4 MPa, 2.8 MPa and 4.2 MPa, the corresponding source flowrate of pump is given in Fig. 15.

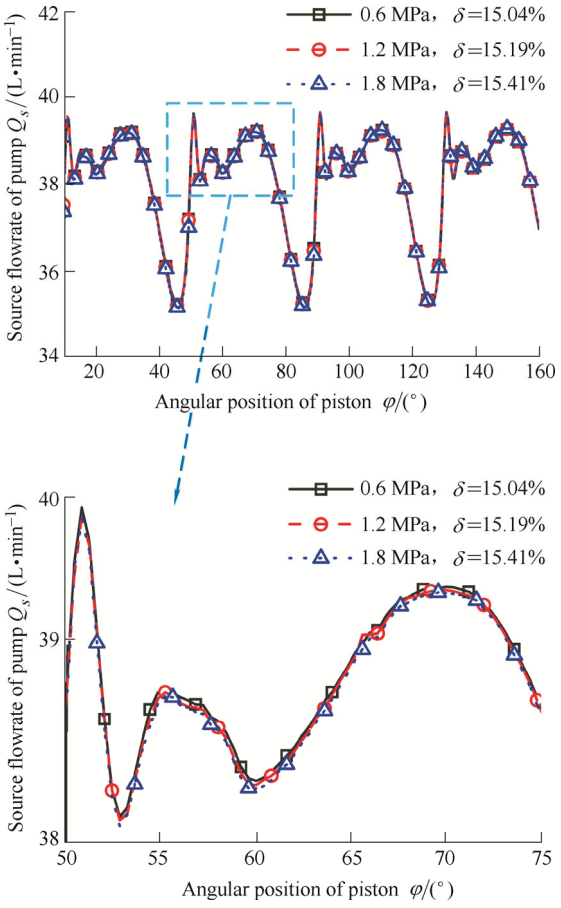

Fig. 14. Source flowrate with respect to different pulsating amplitude of delivery pressure, low-pressure case, 15 MPa

In Fig. 14, the corresponding test accuracy of source flowrate respectively reaches 98.99%, 97.99% and 96.51%. And in Fig. 15, the corresponding test accuracy reaches 98.37%, 98.28% and 96.20%. As Fig. 14 and Fig. 15 show, when the pulsating amplitude of pressure respectively remains ±2%, ±4% and ±6% of the mean pressure, correspondingly the attainable test accuracy of source flowrate of pump can approximately reach a value between 98.37%–98.99%, 97.99%–98.28% and 96.20%–96.51%.

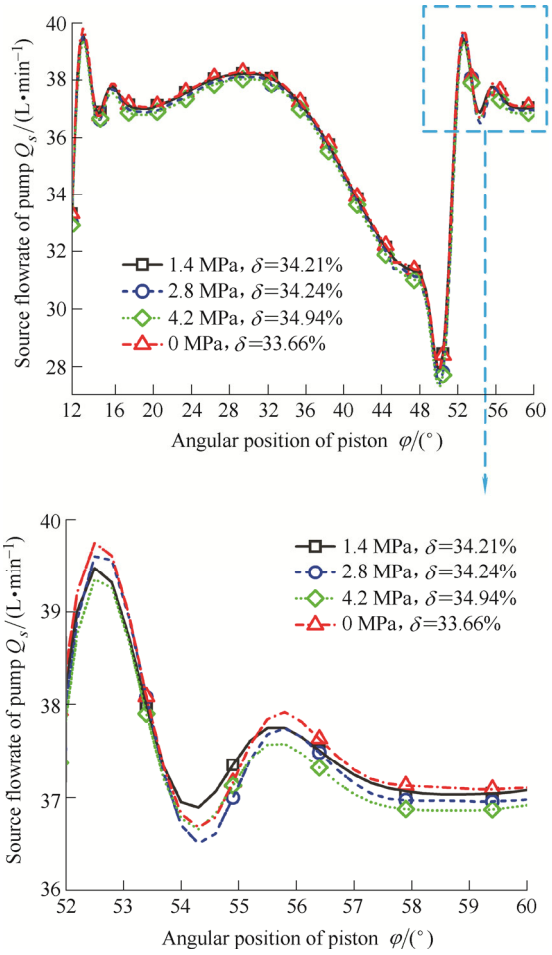

Fig. 15. Source flowrate with respect to different pulsating amplitude of delivery pressure, high-pressure case, 35 MPa

4.2.2 Effect of pressure varying instantaneously

A sudden variation of load yields the instantaneous change of delivery pressure. Generally, the permissible variation rate of pressure for an axial piston pump is less than 1600 MPa/s, nevertheless greater value of variation rate of pressure are considered in this study as well. Fig. 16 shows an instantaneous change of delivery pressure and the corresponding source flowrate of pump. The instantaneous pressure varies from 15 MPa increasing to 18 MPa in three groups of time: 0.003 33 s, 0.004 67 s and 0.006 s, subsequently from 18 MPa decreasing to 15 MPa, the corresponding variation rate of delivery pressure is 901/(−901) MPa/s, 642/(−1508) MPa/s and 500/(−4545) MPa/s.

From Fig. 16, the flowrate decreases with the increasing positive variation rate of pressure in the rising stage of pressure, and increases with the decreasing negative variation rate of pressure in the falling stage of pressure. To sum up, the variation amplitude of flowrate increases with the rise of variation amplitude of change rate of pressure.

In the case that the peak pressure is 18 MPa, 22 MPa and 25 MPa, the duration time hold the same (shown in Fig. 17). The corresponding change rate of pressure is 642/(−1500) MPa/s, 1499/(−3500) MPa/s and 2141/(−5000) MPa/s. The corresponding source flowrate of pump is given in Fig. 17.

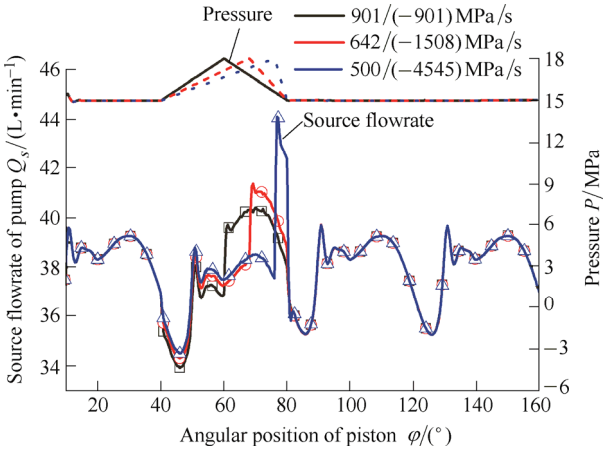

Fig. 16. Instantaneous flowrate with respect to different variation rate of instantaneous change of pressure

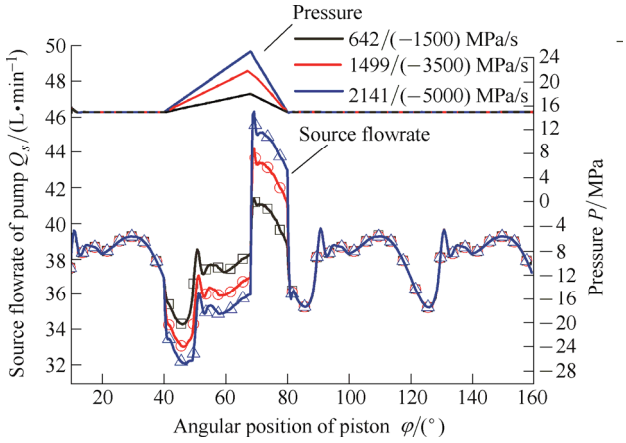

Fig. 17. Instantaneous flowrate with respect to different change rate of instantaneous variation of pressure

Fig. 17 also illustrates that the variation amplitude of flowrate increases with the rise of variation amplitude of change rate of pressure. This is caused by the increasing leakage ripple and the compression ripple due to the variation of pressure and the bulk modulus of compressible hydraulic oil.

4.2.3 Effect of speed varying periodically

In actual working conditions, the speed of pump is not completely constant. There exists frequent variation of speed in small magnitudes. Two cases of this variation are studied as follows.

The assumption in case 1 is that the speed varies with sine regularity, as Eq. (13) shows. The mean speed is 1000 r/min; the corresponding pulsating amplitude is set 20 r/min, 40 r/min and 80 r/min; the frequency is given with the shaft rotational frequency; the initial phase angle is set 0. The corresponding source flowrate of pump is shown in Fig. 18.

As Fig. 18 shows, in the case of speed varying with sine regularity, the peak flowrate and flow pulsation rate increases with the rise of pulsating amplitude of speed. Corresponding to the pulsating amplitude of ±1%, ±2% and ±4% of the mean speed, the test accuracy of source flowrate respectively reaches 96.17%, 94.83% and 89.19%.

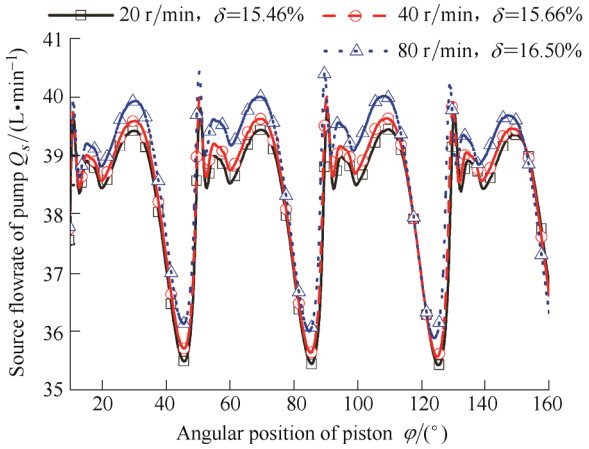

Fig. 18. Source flowrate of pump with respect to different pulsating amplitude of speed

In case 2, it is given that the pump actually works at a constant speed with a small deviation from the desired ideal speed. The ideal speed is set 1500 r/min, and the corresponding actual speed respectively differ ±1% and ±2% from the ideal speed, i.e., 1515 r/min, 1485 r/min, 1530 r/min and 1470 r/min. The source flowrate of pump is shown in Fig. 19.

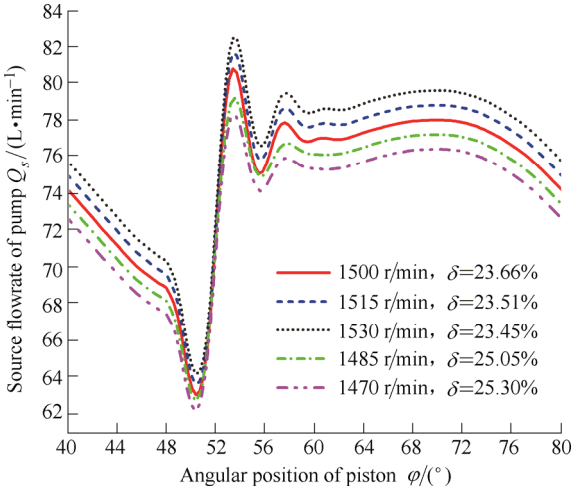

Fig. 19. Source flowrate of pump with respect to different small deviation from the desired ideal speed

Fig. 19 shows that, the variation of flow pulsation rate at the speed differing −1% and −2% from the desired ideal speed is respectively much greater than the flow pulsation rate at the speed differing 1% and 2% from the desired ideal speed. Corresponding to the deviation of ±1% and ±2% from the ideal speed, the test accuracy of the source flowrate can respectively reaches 94.13%–99.37% and 93.07%–99.11%.

Therefore, from Fig. 18 and Fig. 19, in order to guarantee the high test accuracy of the flow ripple, the speed should be held constant as much as possible when testing the flow ripple of pump. For a variation of speed differing within a range of ±2% from the mean speed, the attainable test accuracy of the flow ripple is above 93.07%.

4.2.4 Effect of speed varying instantaneously

The speed has to undergo the transition process between low speed and high speed in some working conditions, such as the start-stop of the pump, or in the variable frequency hydraulic technology, etc. The flow ripple with respect to different variation rate of speed is given in Fig. 20 and Fig. 21, which show that with the rise of variation rate of speed, the pulsating amplitude and mean flowrate increase, resulting in the augment of the flow pulsation rate.

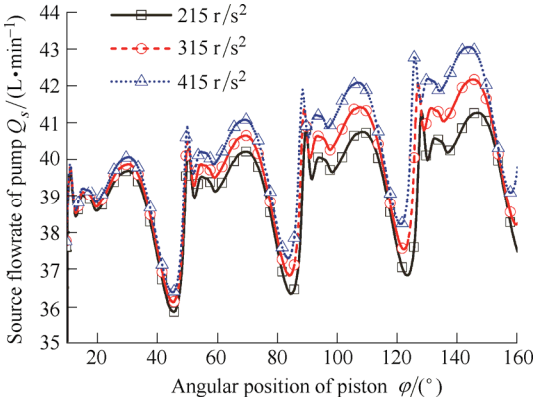

Fig. 20. Flow ripple under different variation rate of speed

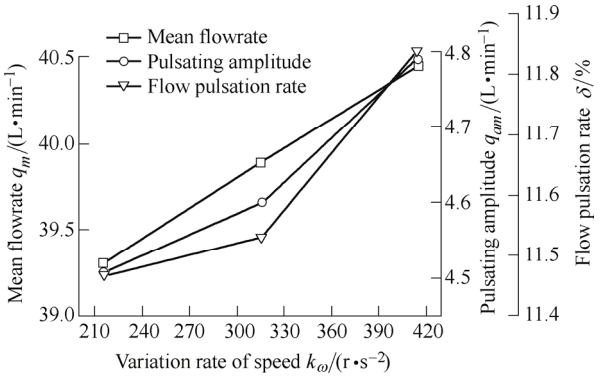

Fig. 21. Evaluation parameters of flow ripple with change rate of speed

5 Conclusions

Based upon the above analysis, it can be concluded that the working conditions have great influence on the flow ripple of axial piston pump and its test accuracy. The derived conclusions are summarized as follows.

(1) The flow pulsating amplitude and flow pulsation rate increase with the rise of delivery pressure, while the minimum flowrate decreases with the rise of delivery pressure. The variation amplitude of flowrate increases with the variation amplitude of change rate of pressure. The angular position of the piston, corresponding to the position where the peak flow ripple is produced, varies with the different delivery pressure.

(2) The minimum flowrate, maximum flowrate and mean flowrate of pump increase with the rise of speed. The flow pulsation rate decreases dramatically with the rise of speed when the speed is less than 27.78% of the maximum speed, subsequently presents a small decrease tendency with the speed further increasing. With the rise of variation rate of speed, the pulsating amplitude and mean flowrate increase, which give rise to the augment of the flow pulsation rate.

(3) With the rise of the swash plate angle, the pulsating amplitude of flow ripple increases, nevertheless the flow pulsation rate decreases.

(4) The maximum flow pulsation rate of pump occurs under the following working conditions: high pressure, low speed and low displacement.

(5) In order to get a high test accuracy of the flow ripple, the speed and delivery pressure should be held constant as much as possible during the test process of the flow ripple. In contrast with the effect of the variation of pressure, the test accuracy is more sensitive to the variation of speed. It makes the test accuracy above 96.20% available for the pulsating amplitude of delivery pressure deviating within a range of ±6% from the mean pressure. However, for a variation of speed deviating within a range of ±2% from the mean speed, the attainable test accuracy of flow ripple is above 93.07%.

References

[1] IVANTYSYNOVA M, HUANG Changchun, CHRISTIANSEN S K. Computer aided valve plate design: An effective way to reduce noise[J]. *SAE Transactions*, 2004, 113(2): 162–173.

[2] IVANTYSYNOVA M, SEENIRAJ G K, HUANG Changchun. Comparison of different valve plate designs focusing on oscillating forces and flow pulsation[C]//*The Ninth Scandinavian International Conference on Fluid Power, SICFP'05*, Linköping University, Sweden, June 1–3, 2005: 62–68.

[3] MANDAL N P, SAHA R, SANYAL D. Theoretical simulation of ripples for different leading-side groove volumes on manifolds in fixed-displacement axial-piston pump[J]. *Proceedings of the Institution of Mechanical Engineers, Part I: Journal of Systems and Control Engineering*, 2008, 222(I6): 557–570.

[4] MANDAL N P, SAHA R, SANYAL D. Effects of flow inertia modelling and valve-plate geometry on swash-plate axial-piston pump performance[J]. *Proceedings of the Institution of Mechanical Engineers, Part I: Journal of Systems and Control Engineering*, 2012, 226(I4): 451–465.

[5] SONG Y C, XU B, YANG H Y. Study on Effect of relief groove angle expressing the position in reducing noise of swash plate axial piston pump[J]. *Advanced Materials and Processes*, 2011, 311–313: 2215–2224.

[6] SEENIRAJ G K. *Model based optimization of axial piston machines focusing on noise and efficiency*[D]. USA: West Lafayette, Indiana, 2009.

[7] NIMAI P, MANDAL R S, DIPANKAR S. Valve plate design of a swash plate type and axial piston pump through theoretical simulation of flow dynamics[C]//*The 7th International Fluid Power Conference*, Aachen University of Technology, Germany, 2010. Aachen: IFK, 2010: 253–259.

[8] GUAN C B, JIAO Z X, HE S Z. Theoretical study of flow ripple for an aviation axial-piston pump with damping holes in the valve plate[J]. *Chinese Journal of Aeronautics*, 2014, 27(1): 169–181.

[9] MANDAL N P, SAHA R, SANYAL D. Theoretical simulation of ripples for different leading-side groove volumes on manifolds in fixed-displacement axial-piston pump[J]. *Proc IMechE, Part I: J. Systems and Control Engineering*, 2008, 222: 557–570.

[10] GUAN C B, JIAO Z X. Dynamic optimization method for valve plate structure of aviation piston pump[J]. *Journal of Beijing*

University of Aeronautics and Astronautics, 2011, 37(3): 274–278.

[11] EDGE K A, DARLING J. The pumping dynamics of swash plate piston pumps[J]. *Journal of Dynamic systems, Measurement and Control*, 1989, 111: 307–312.

[12] MANRING N D. The discharge flow ripple of an axial-piston swash-plate type hydrostatic pump[J]. *Trans. ASME, J. Dynamic Systems, Measmt, and Control*, 2000, 122: 263–268.

[13] MA J E, XU B, ZHANG B, et al. Flow ripple of axial piston pump with computational fluid dynamic simulation using compressible hydraulic oil[J]. *Chinese Journal of Mechanical Engineering*, 2010, 23(1): 45–52.

[14] SHI Z R, PARKER G, GRANSTROM J. Kinematic analysis of a swash-plate controlled variable displacement axial-piston pump with a conical barrel assembly[J]. *Journal of Dynamic Systems Measurement and Control-Transactions of the ASME*, 2010, 132(1): 0110021–0110028.

[15] LEI L, JIAN K, XU J, et al. Discharge flow ripple of axial piston pump with conical cylinder block[J]. *Applied Mechanics and Materials*, 2010, 34–35: 440–445.

[16] MA J E, FANG Y T, XU B, et al. Optimization of cross angle based on the pumping dynamics model[J]. *Journal of Zhejiang University-Science A*, 2010, 11(3): 181–190.

[17] WEI X Y, WANG H Y. The influence of cross angle on the flow ripple of axial piston pumps by CFD simulation[J]. *Advances in Manufacturing Technology*, 2012, 220–223: 1675–1678.

[18] XU B, SONG Y C, YANG H Y. Optimization of swash-plate cross angle noise-reduction structure for swash-plate-type axial piston pump[J]. *Journal of Zhejiang University (Engineering Science)*, 2013, 47(6): 1043–1050. (in Chinese)

[19] ERICSON L, JOHANSSON A, PALMBERG J O. Noise reduction by means of non-uniform placement of pistons in a fluid power machine[C]//*Proceedings of the ASME 2009 Dynamic Systems and Control Conference*, Hollywood, California, USA, October 12–14, 2009, New York: ASME, 2009: 1–8.

[20] MEHTA V S, MANRING N D. Piston pump noise attenuation through modification of piston travel trajectory[C]//*Proceedings of the ASME 2010 International Mechanical Engineering Congress and Exposition (IMECE2010)*, Vancouver, British Columbia, Canada, 2010, New York: ASME, 2010: 1–9.

[21] BERGADA J M, KUMAR S, DAVIES D L, et al. A complete analysis of axial piston pump leakage and output flow ripples[J]. *Applied Mathematical Modelling*, 2012, 36(4): 1731–1751.

[22] XU B, SONG Y C, YANG H Y. Pre-compression volume on flow ripple reduction of a piston pump[J]. *Chinese Journal of Mechanical Engineering*, 2013, 26(6): 1259–1266.

[23] XU B, ZHANG J H, YANG H Y. Simulation research on distribution method of axial piston pump utilizing pressure equalization mechanism[J]. *Proceedings of the Institution of Mechanical Engineers Part C-Journal of Mechanical Engineering Science*, 2013 227(C3): 459–469.

[24] LISELOTT E. Movement of the swash plate in variable in-line pumps at decreased displacement setting angle[C]//*22nd International Congress of Mechanical Engineering (COBEM 2013)*, Ribeirão Preto, SP, Brazil, November 3–7, 2013: 8055–8064.

[25] EDGE K A, JOHNSTON D N. The 'secondary source' method for the measurement of pump pressure ripple characteristics Part 1. Description of method[J]. *Proceedings of the Institution of Mechanical Engineers, Part A. Journal of Power and Process Engineering*, 1990, 204(11): 33–40.

[26] EDGE K A, JOHNSTON D N. The 'secondary source' method for the measurement of pump pressure ripple characteristics Part 2: Experimental results[J]. *Proceedings of the Institution of Mechanical Engineers, Part A. Journal of Power and Energy*, 1990, 204(11): 41–46.

[27] KASSEM S A, BAHR M K. On the dynamics of swash plate axial piston pumps with conical cylinder blocks[C]//*Sixth Triennial International Symposium on Fluid Control Measurement and Visualization*, Sherbrooke University, Sherbrooke, Canada, 2000: 13–17.

[28] JOHANSSON A, ÖVANDER J, PALMBERG J O. Experimental verification of cross-angle for noise reduction in hydraulic piston pumps[J]. *IMechE, Part I: System and Control Engineering*, 2007, 221: 321–330.

[29] ZHANG B, XU B, XIA C L, et al. Modeling and simulation on axial piston pump based on virtual prototype technology[J]. *Chinese Journal of Mechanical Engineering*, 2009, 22(1): 84–90.

[30] XU B, SONG Y C, YANG H Y. Investigation of test principle of flow ripple generated by piston pump with complicated pipe[J]. *Journal of Mechanical Engineering*, 2012, 48(22): 162–167. (in Chinese)

[31] SONG Y C, XU B, YANG H Y, et al. Modified practical approximate method for testing source flow of piston pump[J]. *Journal of Zhejiang University (Engineering Science)*, 2014, 48(2): 200–205. (in Chinese)

[32] ROELANDS C J A. *Correlational aspects of the viscosity-temperature-pressure relationship of lubricating oils*[D]. Druk. U. R. B., Groningen, 1966.

[33] ZHANG B. *Virtual prototype and experimental study on acting oil film of axial piston pump*[D]. Hangzhou: Zhejiang University, 2009.

[34] The International Organization for Standardization, 1996. "ISO 10767-1-1996 Hydraulic Fluid Power - Determination of Pressure Ripple Levels Generated in System and Components. Part 1: Precision method for pumps"[S]. London: British Standards Institution, 1996.

[35] YANG H Y, MA J E, XU B. Research status of axial piston pump fluid-borne noise[J]. *Journal of Mechanical Engineering*, 2009, 45(8): 71–79. (in Chinese)

Biographical notes

XU Bing, born in 1971, is a professor at *State Key Laboratory of Fluid Power Transmission and Control, Zhejiang University, China*. His main research interests include mechatronics control, fluid power components and systems.
E-mail: bxu@zju.edu.cn

HU Min, born in 1985, is currently a PhD candidate at *State Key Laboratory of Fluid Power Transmission and Control, Zhejiang University, China*. His research interests include axial piston pump and energy efficiency.
Tel: +86-15157158489; E-mail: minhu@zju.edu.cn

ZHANG Junhui, born in 1984, obtained his PhD degree from *Zhejiang University, China*, in 2013. His research interests include axial piston pump and fluid born noise control.
Tel: +86-13819156082; E-mail: benzjh@zju.edu.cn